Electronic Supplementary Material (ESI) for Energy & Environmental Science.
This journal is © The Royal Society of Chemistry 2023

Supporting Information

Towards 26% efficiency in inverted perovskite solar cells via interfacial flipped band bending and suppressed deep-level traps

Yiting Zheng[1,2,#], Yaru Li[2,#,], Rongshan Zhuang[1,3], Xueyun Wu[1], Congcong Tian[1], Anxin Sun[1], Chen Chen[2], Yongsheng Guo[2], Yong Hua[3], Ke Meng[2,*], Kai Wu[2,*], Chun-Chao Chen[1,2,*]*

[1]School of Materials Science and Engineering

Shanghai Jiao Tong University

Shanghai 200240, P. R. China

E-mail: c3chen@sjtu.edu.cn

[2]Future Energy Research Institute of Shanghai

Contemporary Amperex Technology Co. Limited (CATL)

Shanghai 200240, P. R. China

E-mail: liyr05@catl.com, mengk01@catl.com, wuk@catl.com

[3]Yunnan Key Laboratory for Micro/Nano Materials & Technology

School of Materials and Energy

Yunnan University

Kunming 650091, P. R. China

Keywords:

inverted perovskite solar cells, deprotonation, energy band bending, deep-level surface traps, nonradiative recombination loss

[#]Contributed equally to this work

[*]Corresponding authors

Experimental Section

Materials

Formamidine iodide (FAI, >99.5%), methylammonium iodide (MAI, >99.5%) and methylammonium chloride (MACl, >99.5%) were gained from Greatcell Solar Materials Pty Ltd., Lead (II) iodide (PbI_2, >99.99%) was purchased form Xi'an E-Light New Material Co., Ltd. Cesium iodide (CsI, >99.99%), [4-(3,6-dimethyl-9H-carbazol-9-yl)butyl]phosphonic acid (Me-4PACz), piperazinium diiodide (PDI), C_{60} and bathocuproine (BCP) were purchased from Xi'an Polymer Light Technology Crop. N, N Dimethylformamide (DMF, 99.8%), Dimethyl sulfoxide (DMSO, 99.8%) and chlorobenzene (CB) were obtained from Sigma-Aldrich. All materials used directly after purchase without further processing.

Device fabrication

The FTO substrates (2.0*2.0 cm^2) were sequentially washed with deionized water, absolute ethanol, acetone and isopropanol in ultrasonic bath for 20 min. Then, the FTO substrates were further cleaned via UV-Ozone treatment for 15 min. After cooling to room temperature, the Me-4PACz (1 mmol in methanol) was spin-coated on the substrates at 5000 rpm 30 s and annealed at 100 °C 10 min.

The perovskite precursor solution was prepared by dissolving FAI, MAI, CsI, and PbI_2 in anhydrous DMF: DMSO=4: 1 (v: v) according to the stoichiometric formula of 1.5 M $Cs_{0.05}(FA_{0.98}MA_{0.02})_{0.95}PbI_3$, with 20 mol% MACl. The solution was stirred at room temperature until dissolved and filtered through a polytetrafluoroethylene (PTFE) filter (0.22 μm) before use. Then, 150 μL perovskite precursor solution was dropped onto

Me-4PACz substrates, spin-coated at 2000 rpm for 25 s and 5000 rpm for 30 s. The 200 μL of chlorobenzene was poured on the substrates 10 s prior to the end of the program. Then, quickly transferred the substrates to annealing at 110 °C for 20 min. The supernatant of PDI saturated solution was spin-coated at 5000 rpm for 30 s on the upper surface of the annealed perovskite films, and then transferred to a hot stage of 100 °C annealing for 10 min. Then, The C_{60} (27 nm) and BCP (7 nm) were sequentially deposited on the perovskite films by vacuum evaporation. Finally, Cu (120 nm) was deposited as back electrode through a mask (the effective area of the electrode is 0.075 cm^2) by thermal evaporation under 9×10^{-5} Pa.

First-principles calculations

We performed the first-principles calculations in the frame of density functional theory (DFT) with the Vienna ab initio simulation package (VASP).[1] The exchange-correlation energy is described by the Perdew-Burke-Ernzerhof (PBE) form of generalized-gradient approximation (GGA) exchange-correlation energy functional.[2] The structure optimizations of systems of PD^+ ion before and after adsorption on PbI_2 terminal $FAPbI_3$ (100) surfaces with I vacancy and I interstitial defects have been carried out by allowing top layer atomic positions to vary and fixing lattice parameters and bottom layer atomic positions until the energy difference of successive atom configurations was less than 10^{-6} eV. The force on each atom in the relaxed structures was less than 0.015 eV/Å. The cutoff energy for the plane-wave basis set was set to 400 eV. The k-point spacing was set to be smaller than 0.03 $Å^{-1}$ over Brillouin zone (BZ).[3]

To calculate the deprotonation energy of PD^+, FA^+ and MA^+ ions, they were put in 10 Å*10 Å*10 Å lattice. Their structure optimizations were performed by relaxing atomic positions and fixing lattice parameters.

Characterization

The ^1H NMR spectra were tested by 600 MHz nuclear magnetic resonance spectrometer (Avance III). X-ray photoelectron spectra (XPS) were acquired on an AXIS Ultra DLD X-ray photoelectron spectrometer and calibrated based on the C 1s peak (284.8 eV). Ultraviolet photoelectron spectroscopy (UPS) was measured by AXIS Ultra DLD machine. The SEM images were obtained by field emission scanning electron microscopy (JSM-7800F). Atom force microscopy (AFM) images were observed on the Bruke Bio-FastScan AFM using taping mode. X-ray diffraction (XRD) patterns were taken on a D8 Advance X-ray diffractometer with Cu Ka radiation as the X-ray source with a scan rate of 8º min^{-1}. The grazing incidence wide angle X-ray scattering (GIWAXS) spectra were obtained at beamline BL16B1 in the Shanghai Synchrotron Radiation Facility (SSRF) and the incidence angle of the X-ray beam was 0.4º. The PL quantum yield (PLQY), Steady state photoluminescence (PL) and time-resolved photoluminescence (TRPL) were carried out using FLS 1000 photoluminescence spectrometer. PL mapping images were obtained by Raman image-scanning electron microscope (RISE-MAGNA) with scanning area of 50*50 um^2. Time-of-flight secondary ion mass spectra (ToF-SIMS) were detected by ION TOF ToF SIMS 5-100 (Primary ion beam: Bi^{3+}, 30 keV, incident angle: 45 deg, scanning area: 150*150 um^2, pixel: 128*128, beam current: 0.48 pA). The transient photovoltage (TPV) and transient

photocurrent (TPC) curves are detected by Fluxim Paios Spectrometer. The current density-voltage (*J-V*) curves of the device is measured under AM 1.5G illumination at 100 mW cm^{-2} (calibrated with a standard Si solar cell) using an Abet Technologies Sun 2000 solar simulator and a Keithley 2400 source meter.

Femtosecond transient absorption (fs-TA)

The pump of fs-TA spectroscopy with broadband capabilities and 1 fs resolution is frequency-doubled to 400 nm. The probe pulses are generated by passing another fraction of the 800 nm pulses through the 2 mm thick sapphire crystal. Before white light generation, the 800 nm amplifed pulses are passed through a motorized delay stage. The delay interval is 1 ms. Depending on the movement of delay stage, the transient species are detected at different time scales following excitation. In order to reduce the error, the same detection light intensity is controlled, background processing is carried out and the number of integrations is adjusted to 2000 times before each sample test. The fluence of the pump pulse (~2.67 μJ/cm^2) is calculated by the excitation beam spot size (diameter) ~0.08 cm. For hot carrier temperature calculation, the high energy tail of the TA spectrum can be approximately described by the Maxwell-Boltzmann distribution function:[4,5]

$$\Delta A[E] \propto e^{-\frac{E - E_f}{k_B T_c}} \#(1)$$

Where, E_f is the quasi-Fermi energy and k_B is the Boltzmann constant. The carrier temperature (T_c) can thus be obtained by fitting the high energy tail using the above equation. To ensure that the hot carriers have reached a quasi-equilibrium via the carrier-carrier scattering after the initial fs-pulse excitation, the hot carrier temperatures

are analyzed from TA spectra after 0.5 ps time delay.

Calculation of quasi-Fermi level splitting (QFLS) and $\Delta V_{oc-imp}^{nonrad}$ recombination loss

QFLS can be calculated from PLQY by the following formula:[6]

$$QFLS = QFLS_{rad} + K_B T ln(PLQY) = K_B T ln\left(\frac{J_G}{J_{0,rad}} \times PLQY\right) \#(2)$$

Where, $QFLS_{rad}$ is the radiation limit of semiconductor materials, which sets the maximum achievable splitting of the quasi-Fermi level without considering nonradiative radiation recombination. K_B is the Boltzmann constant, J_G is the photogenerated current density, $J_{0,rad}$ is the dark state radiative recombination saturation current density. According to the detailed balance theory, the $J_{0,rad}$ can be calculated by the following equations:[6]

$$J_{0,rad} = q\int_0^\infty EQE_{PV}(E)\phi_{BB}(E)dE \#(3)$$

$$\phi_{BB}(E) = \frac{2\pi E^2}{h^3 c^2} \frac{1}{\exp\left(\frac{E}{K_B T}\right) - 1} \#(4)$$

Where q is the elementary charge, EQE_{PV} is the photovoltaic external quantum efficiency, ϕ_{BB} is the black-body radiative spectrum, E is the photo energy, h is the Planck constant, and c is the light speed in vacuum. The calculated $QFLS_{rad}$ is 1.286 eV. Finally, $\Delta V_{oc-imp}^{nonrad}$ recombination loss can be calculated from PLQY by the following formula:

$$\Delta V_{oc-imp}^{nonrad} = -K_B T \ln \frac{(PLQY)}{q} \#(5)$$

Finally, the calculated QFLS and $\Delta V_{oc-imp}^{nonrad}$ of different samples are shown in Table 1.

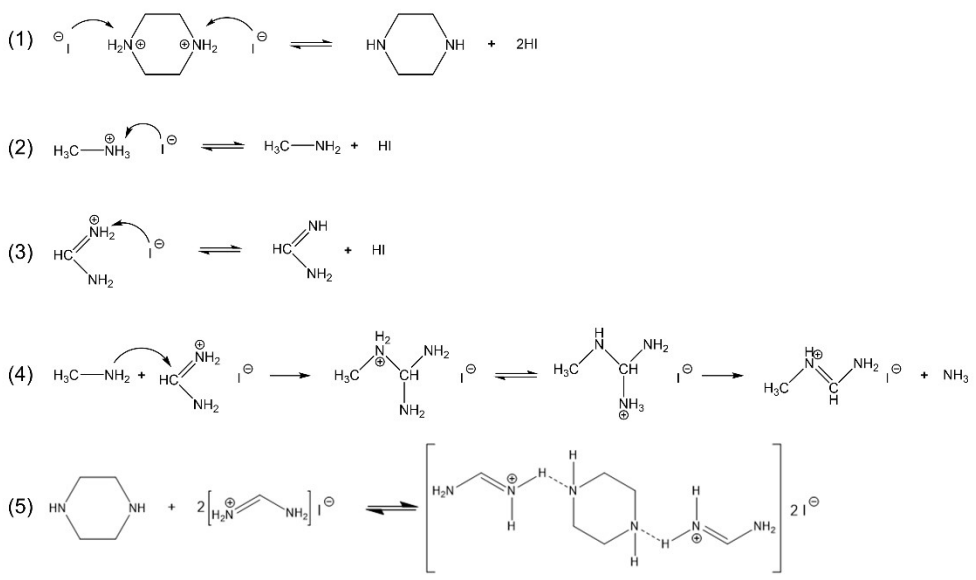

Scheme S1. Deprotonation of (1) PDI, (2) MAI and (3) FAI. After DFT calculation, the deprotonation energy of PDI is -3.326 eV, while that of FAI and MAI are -1.612 eV and -1.854 eV, indicating that PDI is more prone to deprotonation thermodynamically. (4) The amine-cation reactions between MA and FA^+ to generate MFA^+. (5) Piperazine forms a complex with FAI through hydrogen bonding.

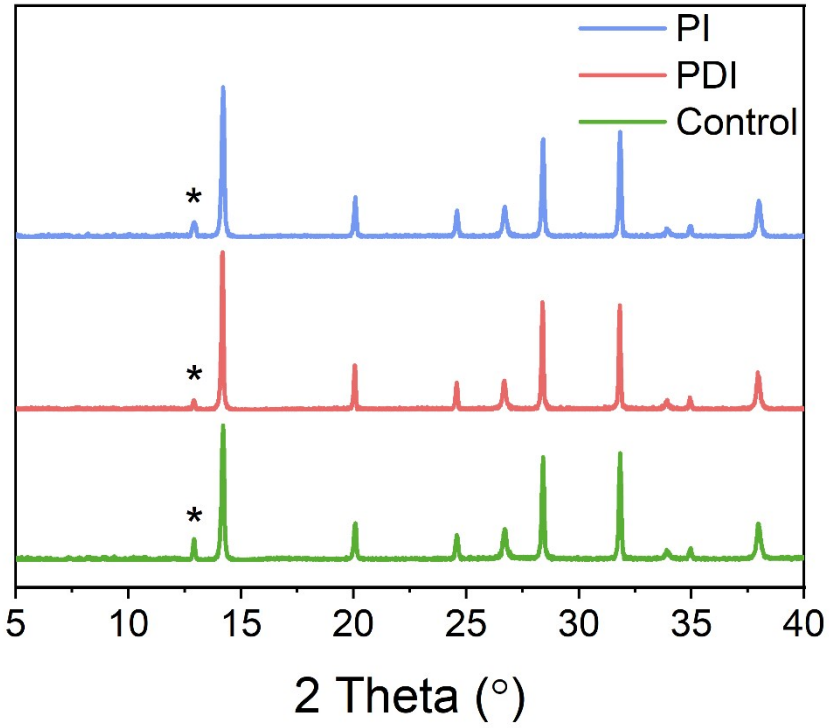

Fig. S1. XRD spectra of Control, PDI-treated and PI-treated perovskite films. * denoted PbI_2.

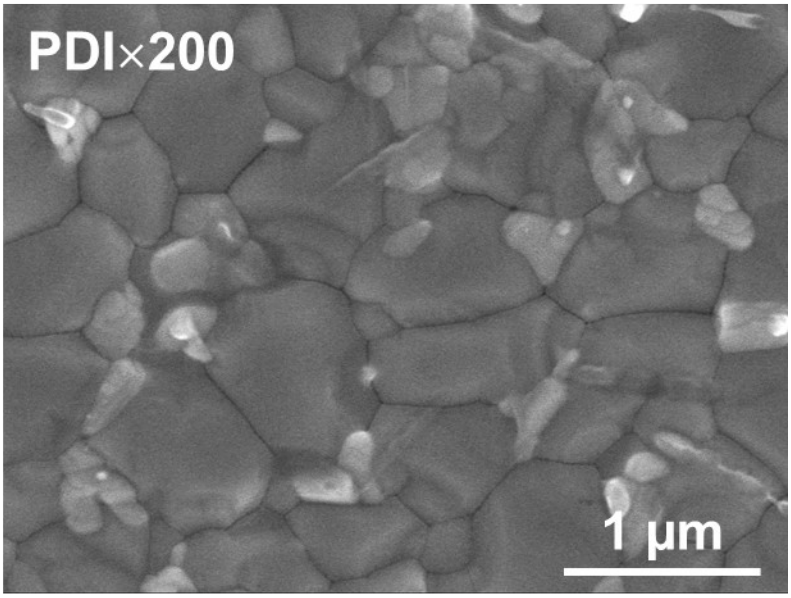

Fig. S2. Top-view SEM image of perovskite film after PDI treatment for 200 times.

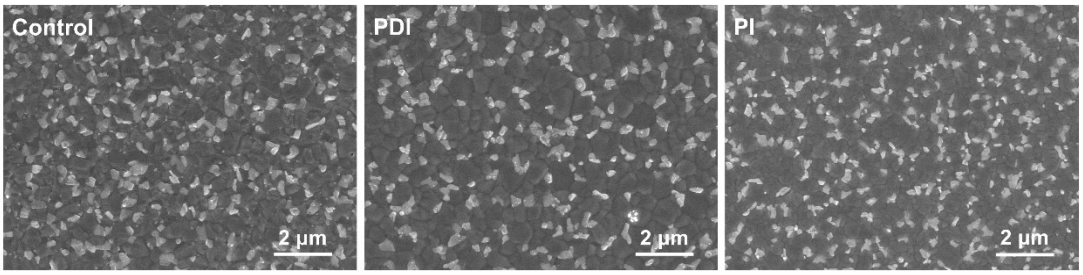

Fig. S3. Top-view SEM images of Control, PDI-treated and PI-treated perovskite films.

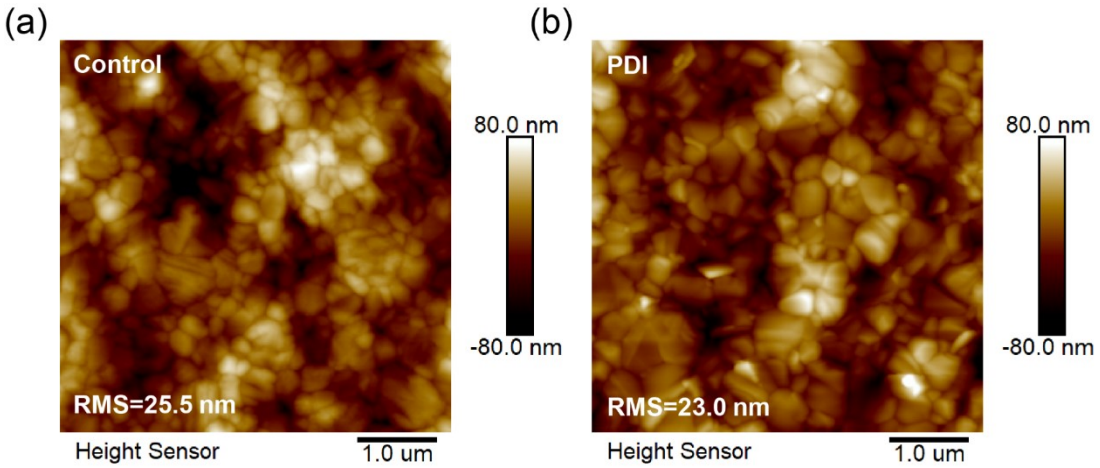

Fig. S4. AFM images of Control and PDI-treated perovskite films.

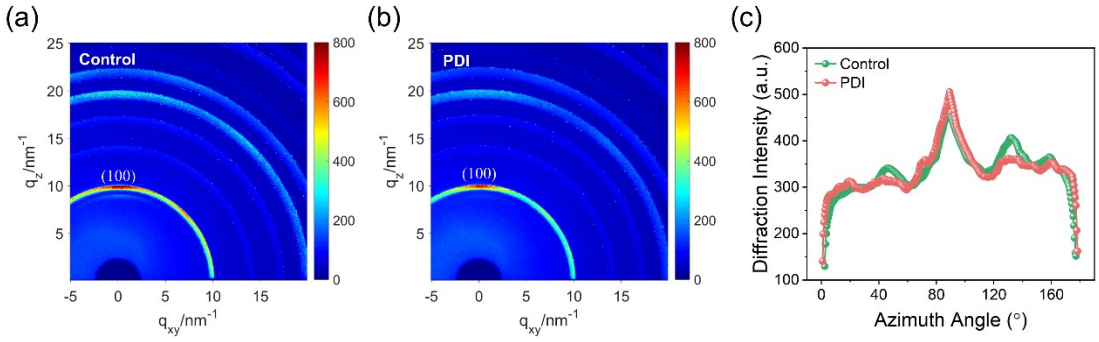

Fig. S5. 2D GIWAXS patterns of (a) Control and (b) PDI-treated perovskite films. (c) Azimuthally integrating scattering intensity along the ring at q=10 nm^{-1} of Control and PDI-treated perovskite films.

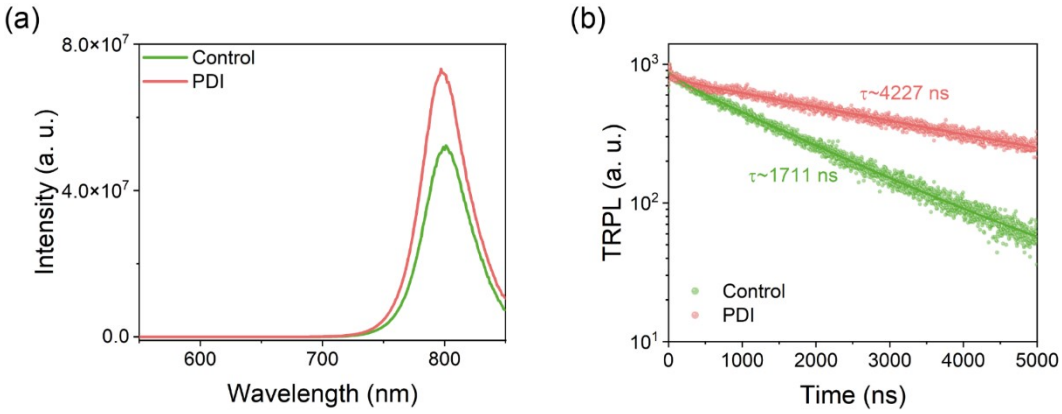

Fig. S6. (a) Steady state PL and (b) TRPL decays of the Control and PDI perovskite films.

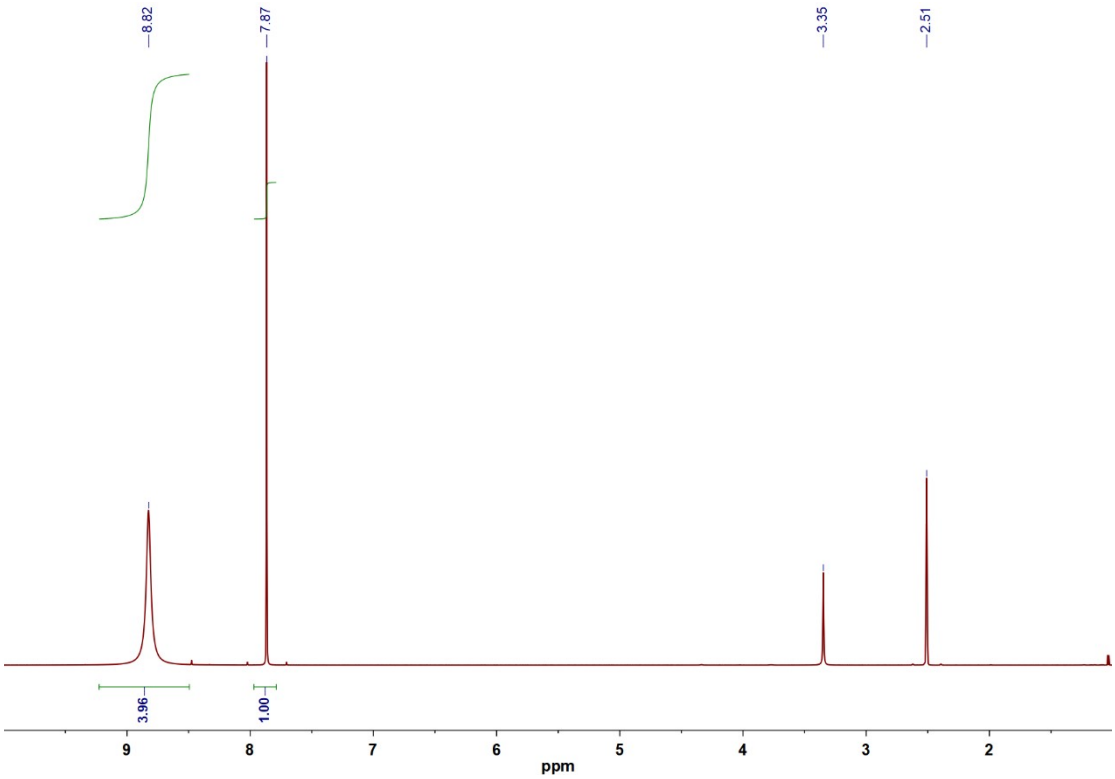

Fig. S7. The full ^{1}H NMR spectra of FAI in DMSO-d6. ^{1}H signals of δ~2.5 ppm and 3.3 ppm are attributed to H_2O and DMSO-d6.

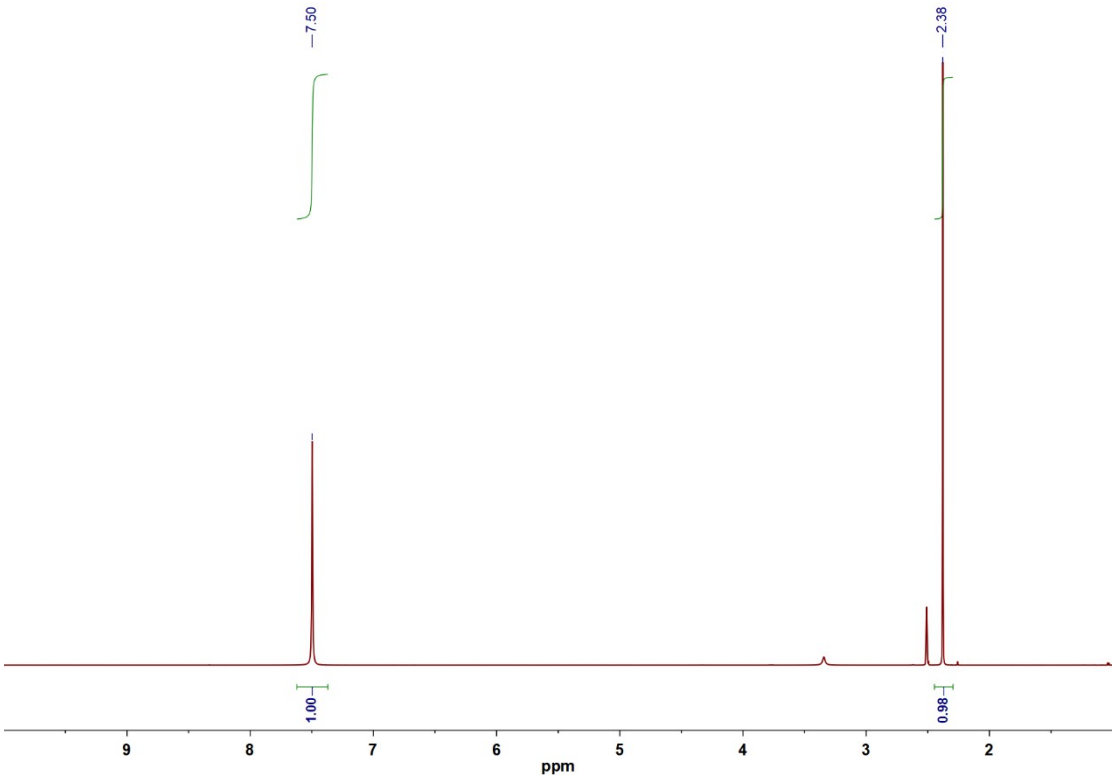

Fig. S8. The full ^{1}H NMR spectra of MAI in DMSO-d6.

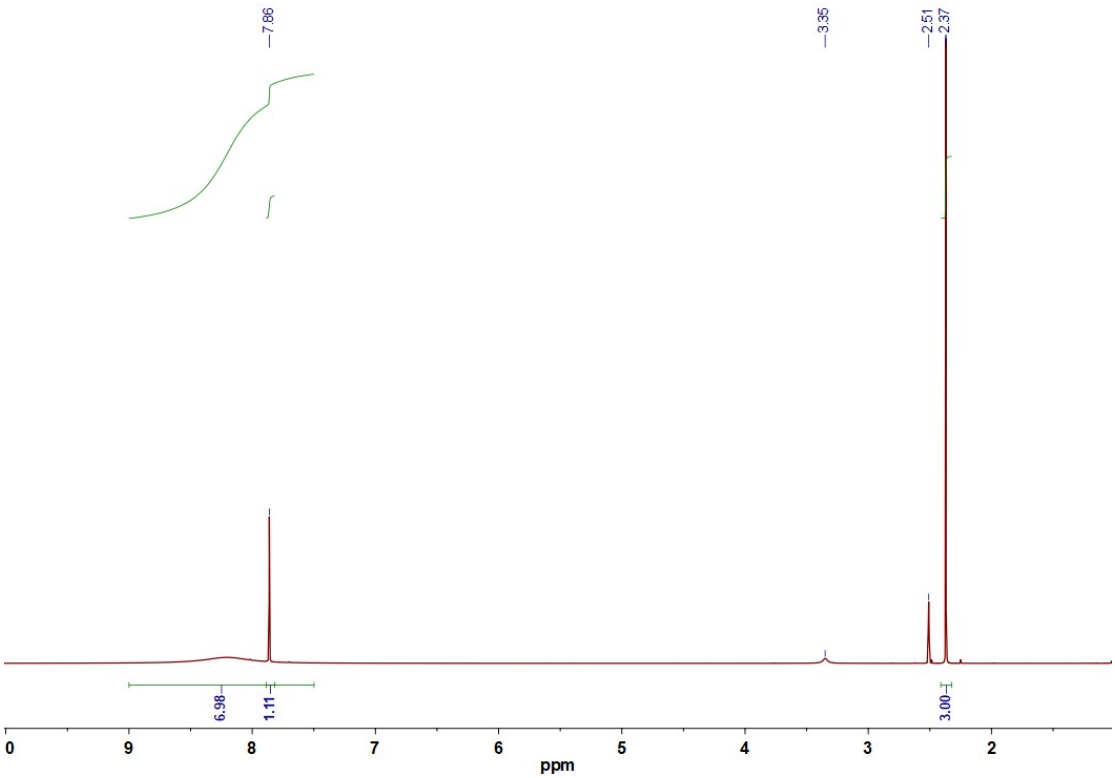

Fig. S9. The full ^{1}H NMR spectra of FAI+MAI+PbI_2 in DMSO-d6 aging for 1 h at 60 ^{o}C.

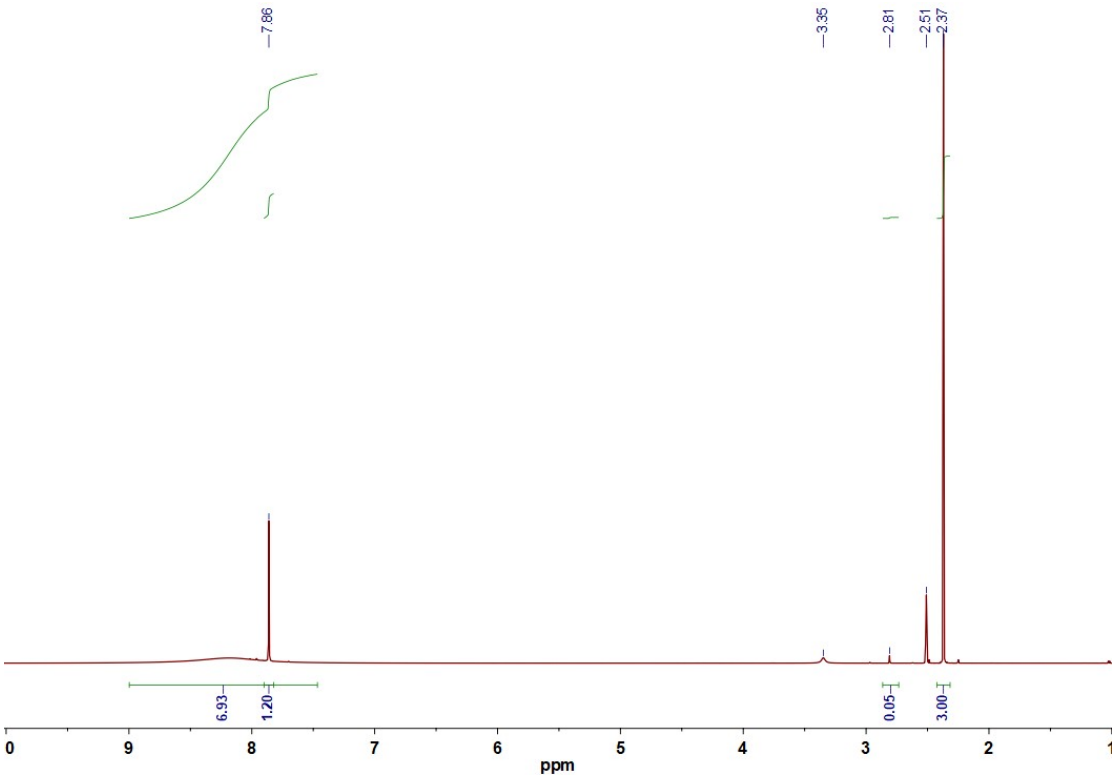

Fig. S10. The full ^{1}H NMR spectra of FAI+MAI+PbI_2 in DMSO-d6 aging for 48 h at 60 ºC. A new peak at δ=2.81 ppm appeared in the perovskite solution, which was attributed to MFAI.

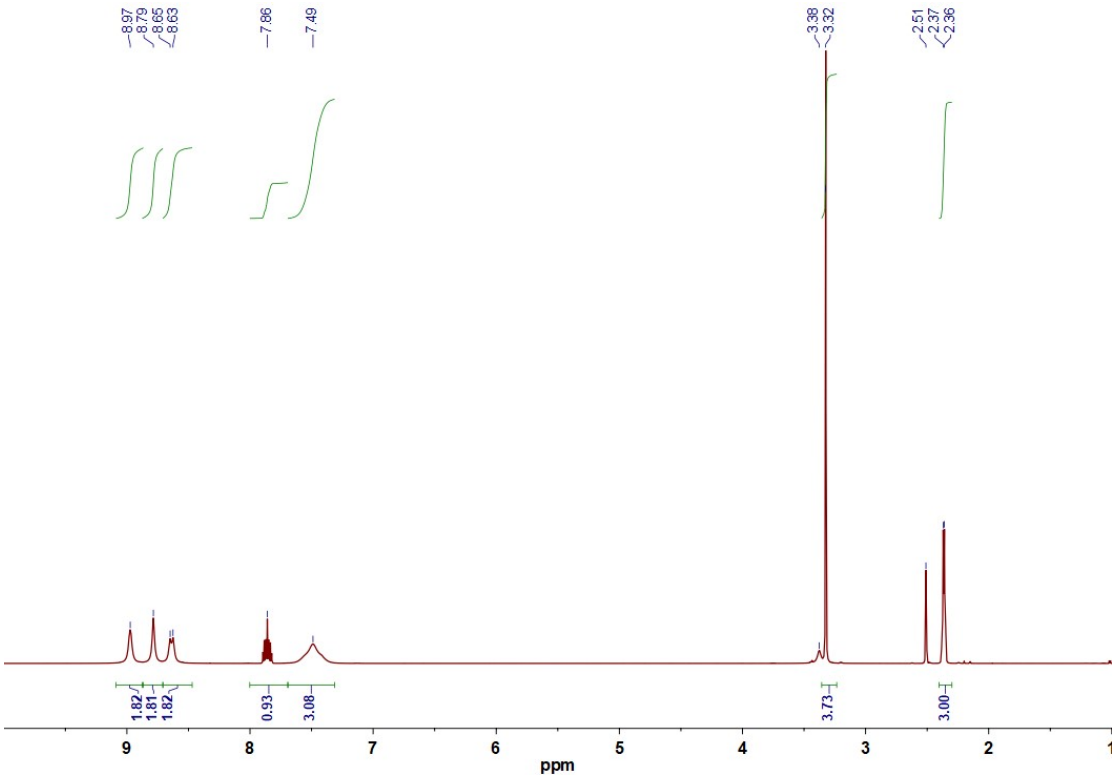

Fig. S11. The full ^{1}H NMR spectra of PDI+FAI+MAI+PbI_2 in DMSO-d6 aging for 1 h at 60 ºC.

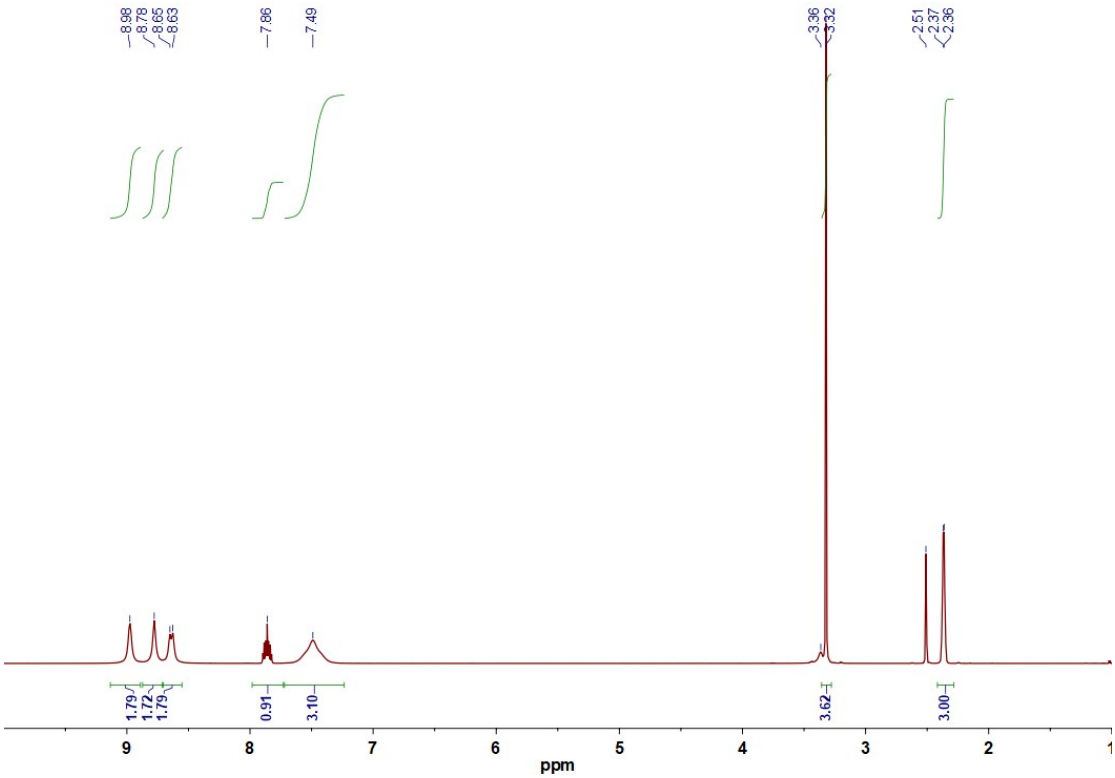

Fig. S12. The full ^{1}H NMR spectra of PDI+FAI+MAI+PbI_2 in DMSO-d6 aging for 48 h at 60 ºC.

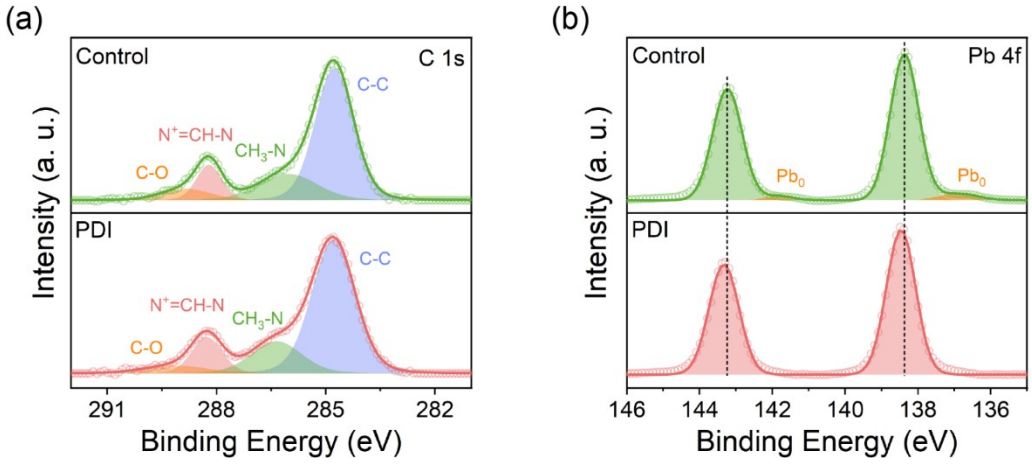

Fig. S13. XPS spectra of (a) C 1s and (b) Pb 4f of Control and PDI-treated perovskite films.

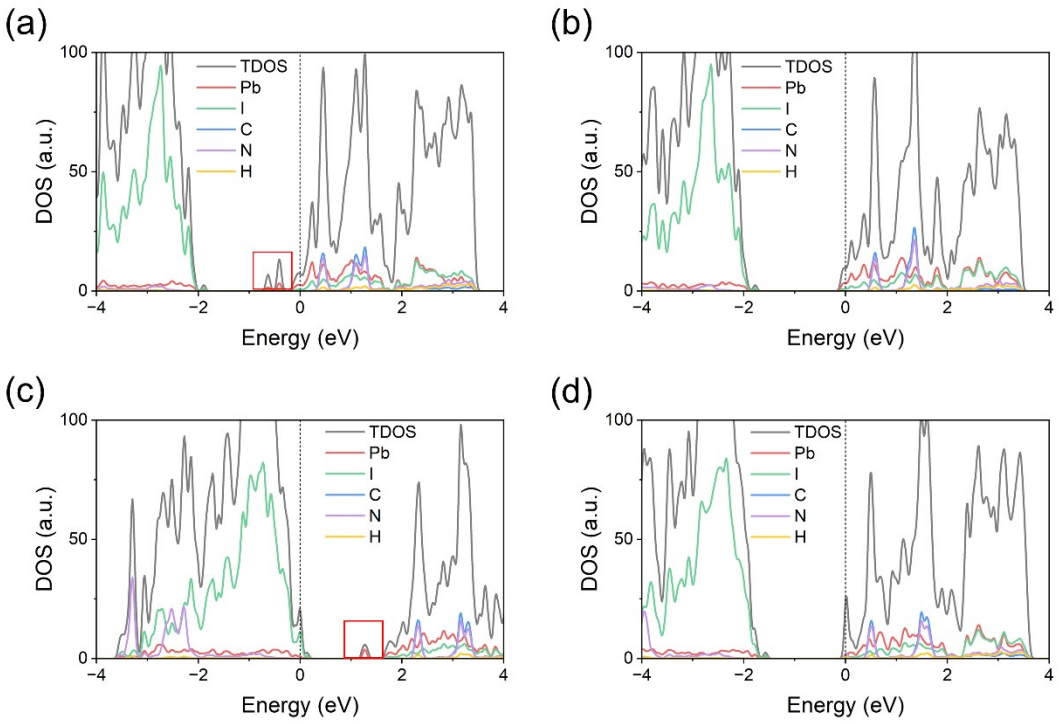

Fig. S14. Density of states of perovskites with iodine vacancies (a) before and (b) after PDI treatment, and iodine interstitials (c) before and (d) after PDI treatment.

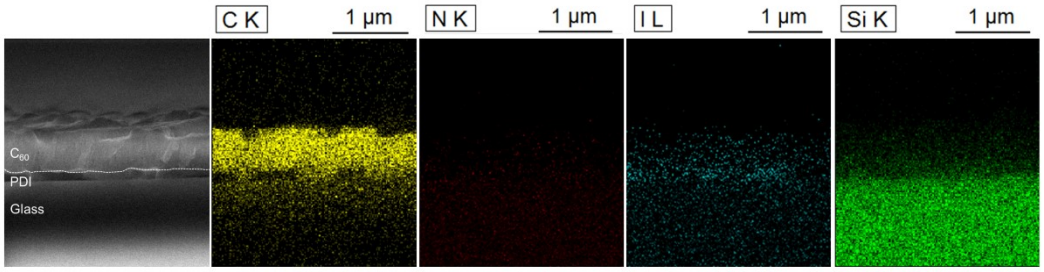

Fig. S15. Cross-section SEM and EDS images of PDI/C_{60} stack.

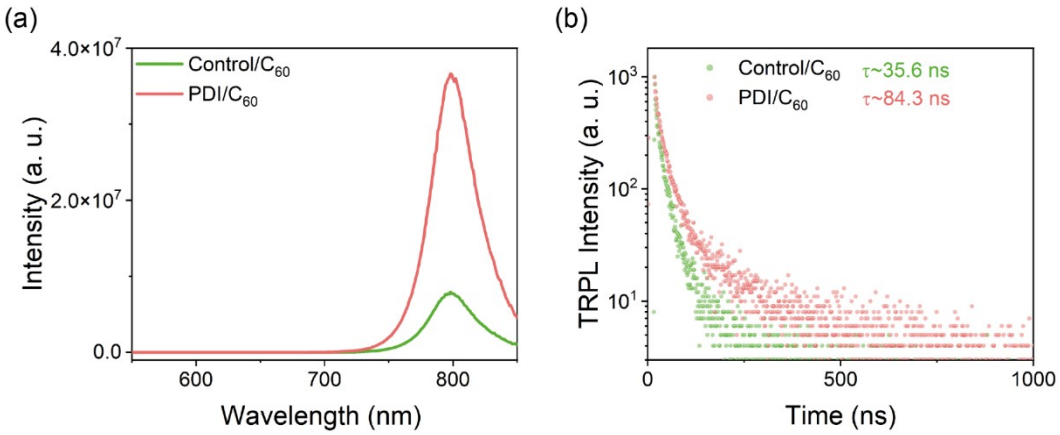

Fig. S16. (a) Steady state PL and (b) TRPL decays of the Control/C60 and PDI/C60 samples.

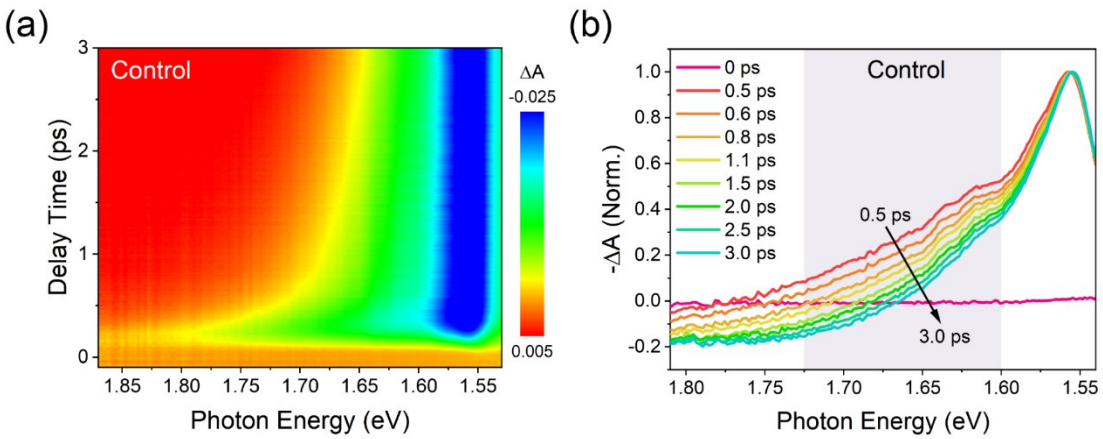

Fig. S17. (a) The pseudo color plot and (b) normalized pump-probe fs-TA spectra of Control perovskite films.

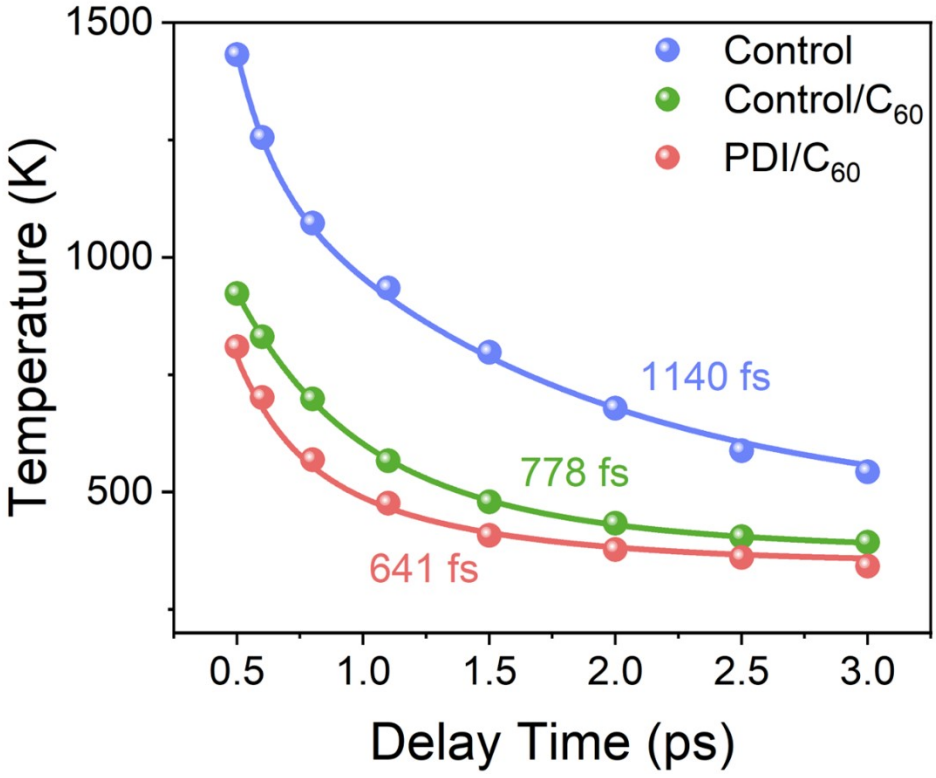

Fig. S18. Extracted hot carrier temperatures with delay time for Control, Control/C_{60} and PDI/C_{60} samples.

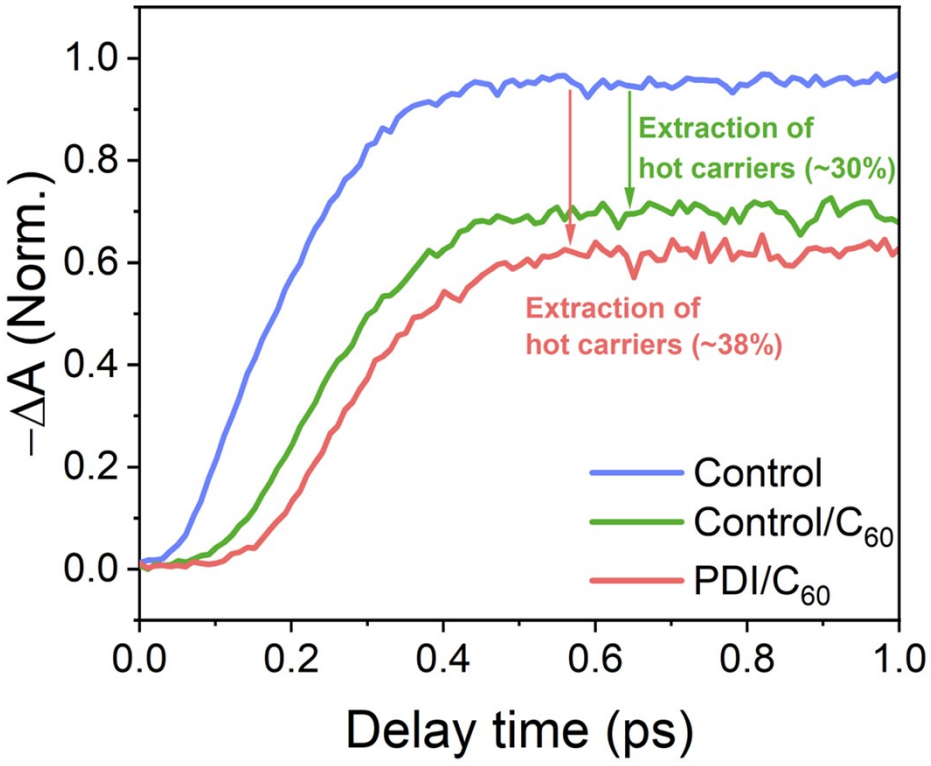

Fig. S19. Absolute bleach amplitude at early delay time at 3.1 eV excitation of Control, Control/C_{60} and PDI/C_{60} samples.

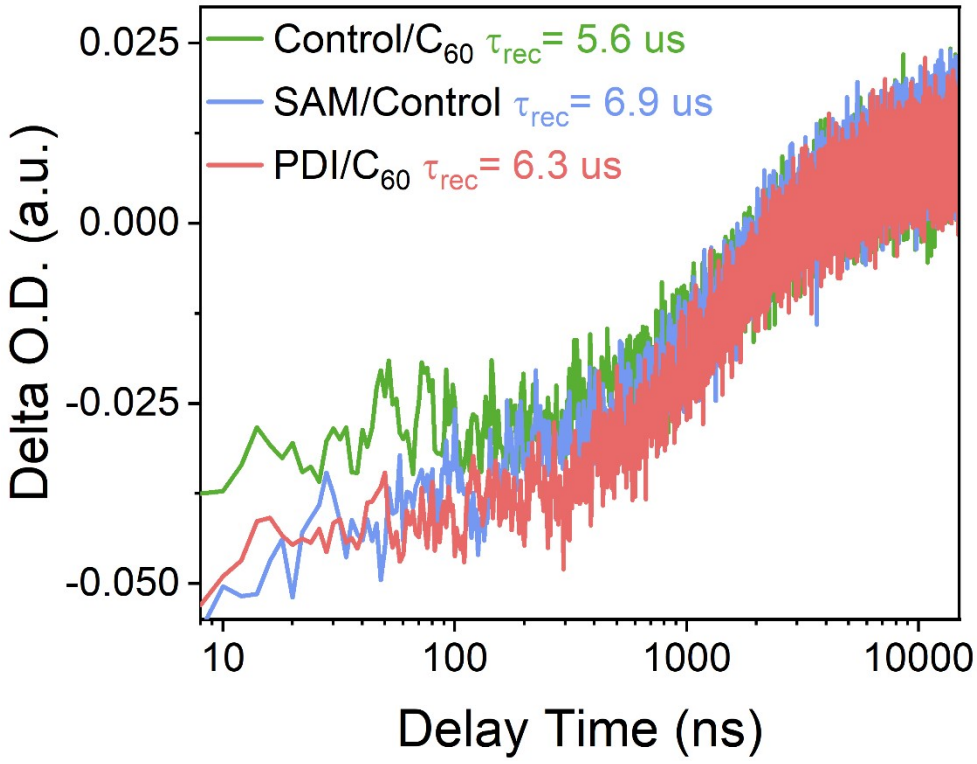

Fig. S20. Nanosecond transient absorption dynamics for Control/C_{60}, SAM/Control and PDI/C_{60} samples.

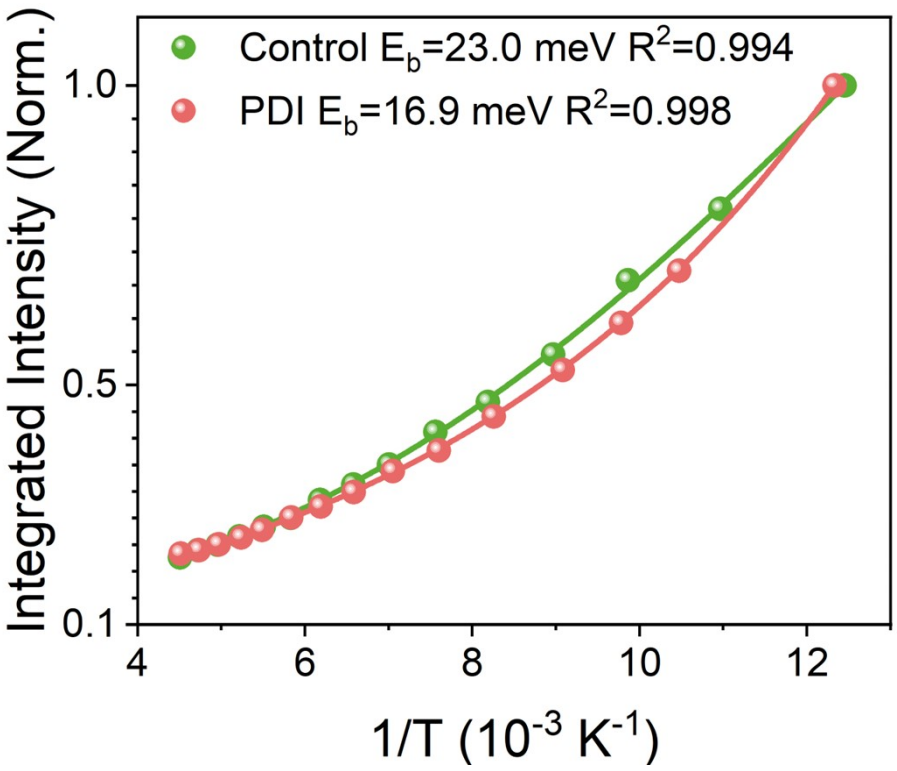

Fig. S21. Relevant integration of the temperature-dependent PL intensity of control and PDI-treated perovskite film and fitting curves for E_b.

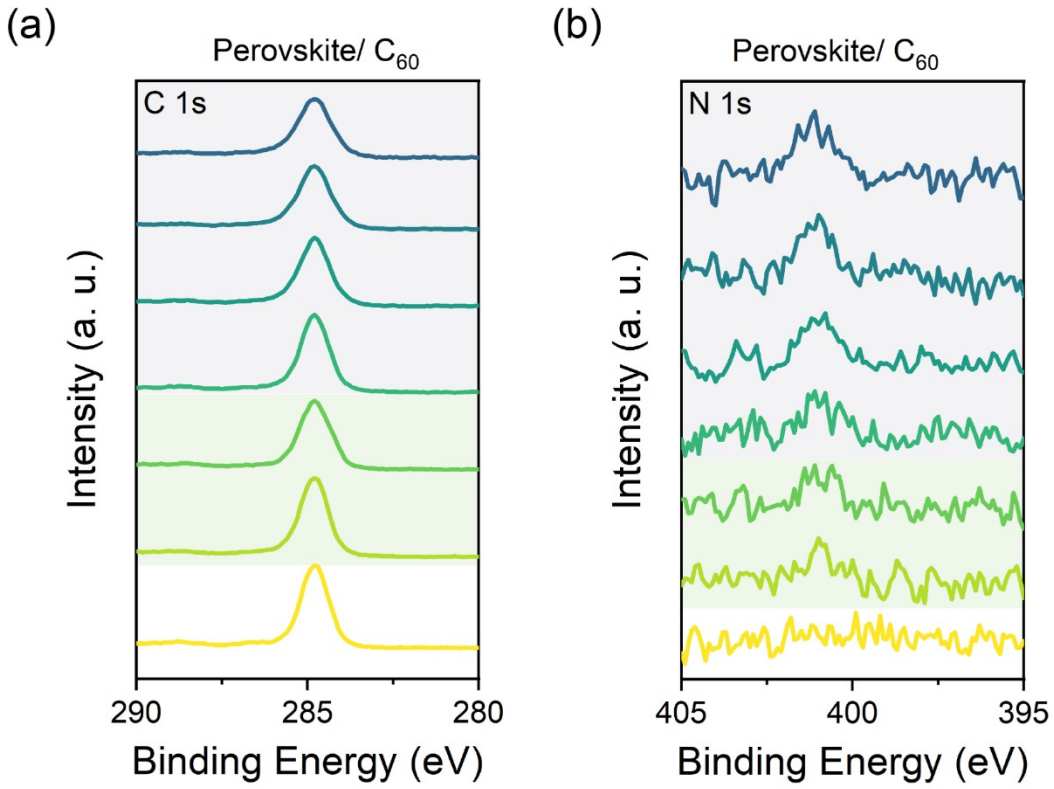

Fig. S22. Depth profiling XPS spectra of C 1s and N 1s for perovskite/C_{60} stack with etching time.

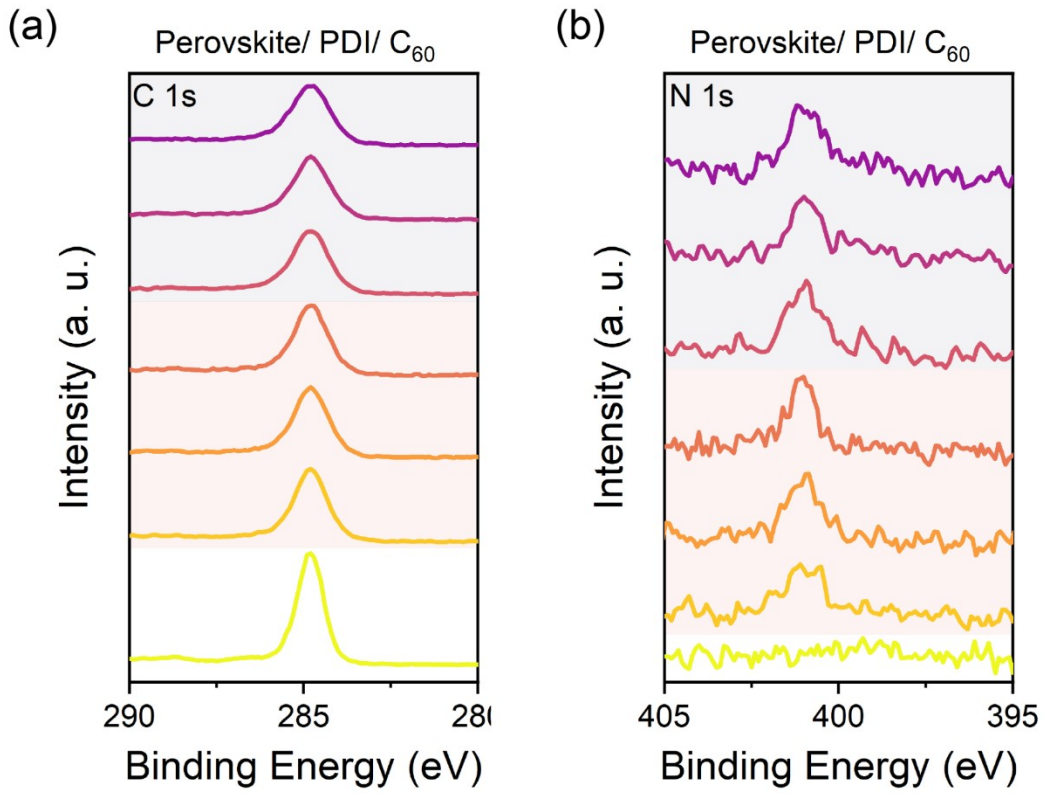

Fig. S23. Depth profiling XPS spectra of C 1s and N 1s for perovskite/PDI/C_{60} stack with etching time.

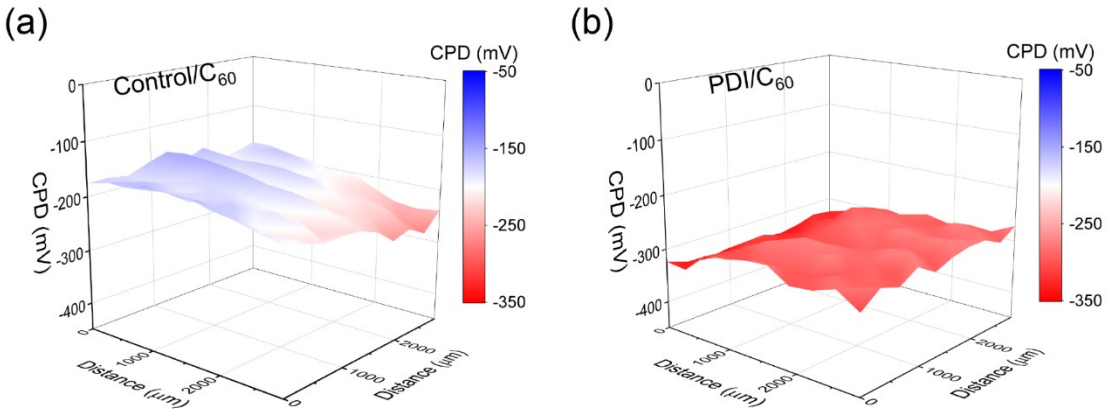

Fig. S24. Surface contact potential of Control and PDI-treated PSCs.

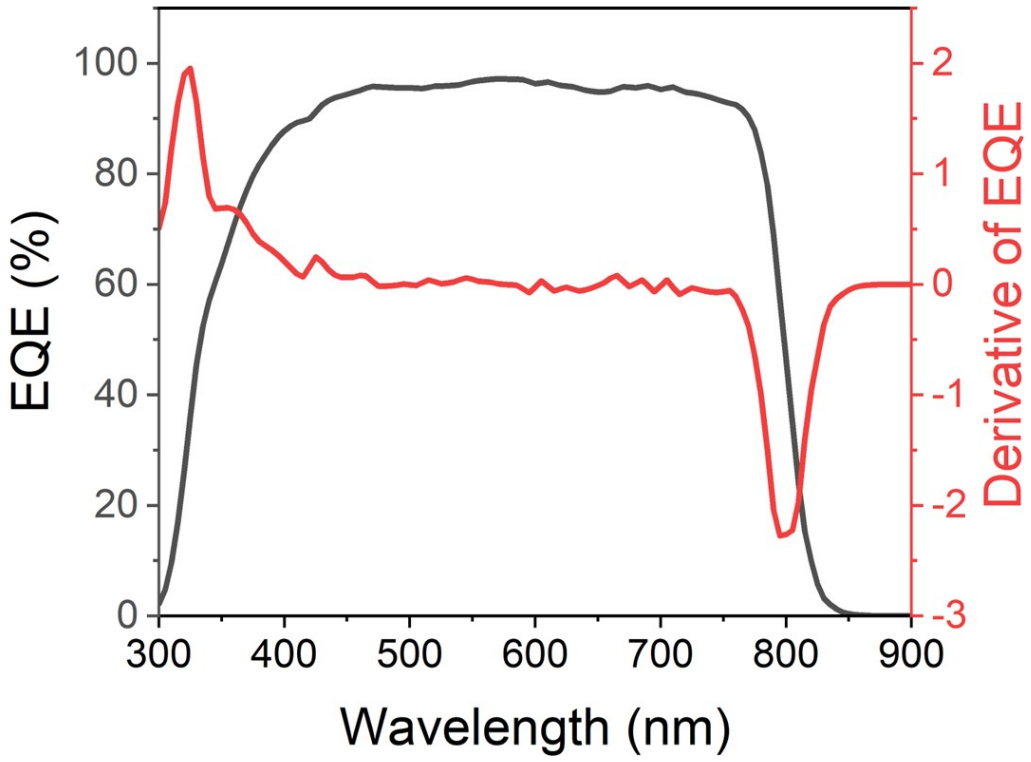

Fig. S25. Analysis of perovskite bandgap from the EQE spectrum by taking its derivative spectrum. The bandgap was estimated to be about 1.55 eV.

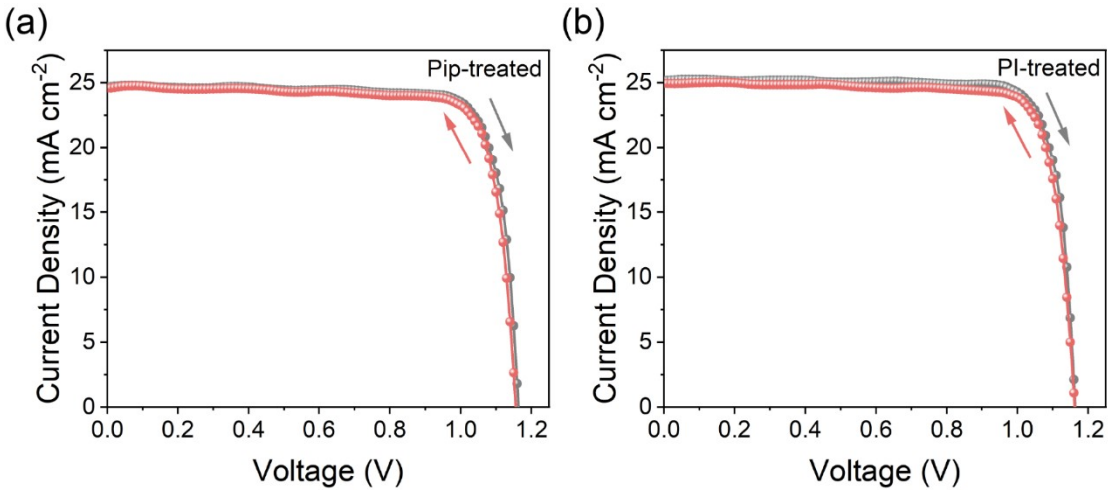

Fig. S26. *J-V* curves of Pip- and PI-treated devices with 0.075 cm^2 in reverse scan and forward scan.

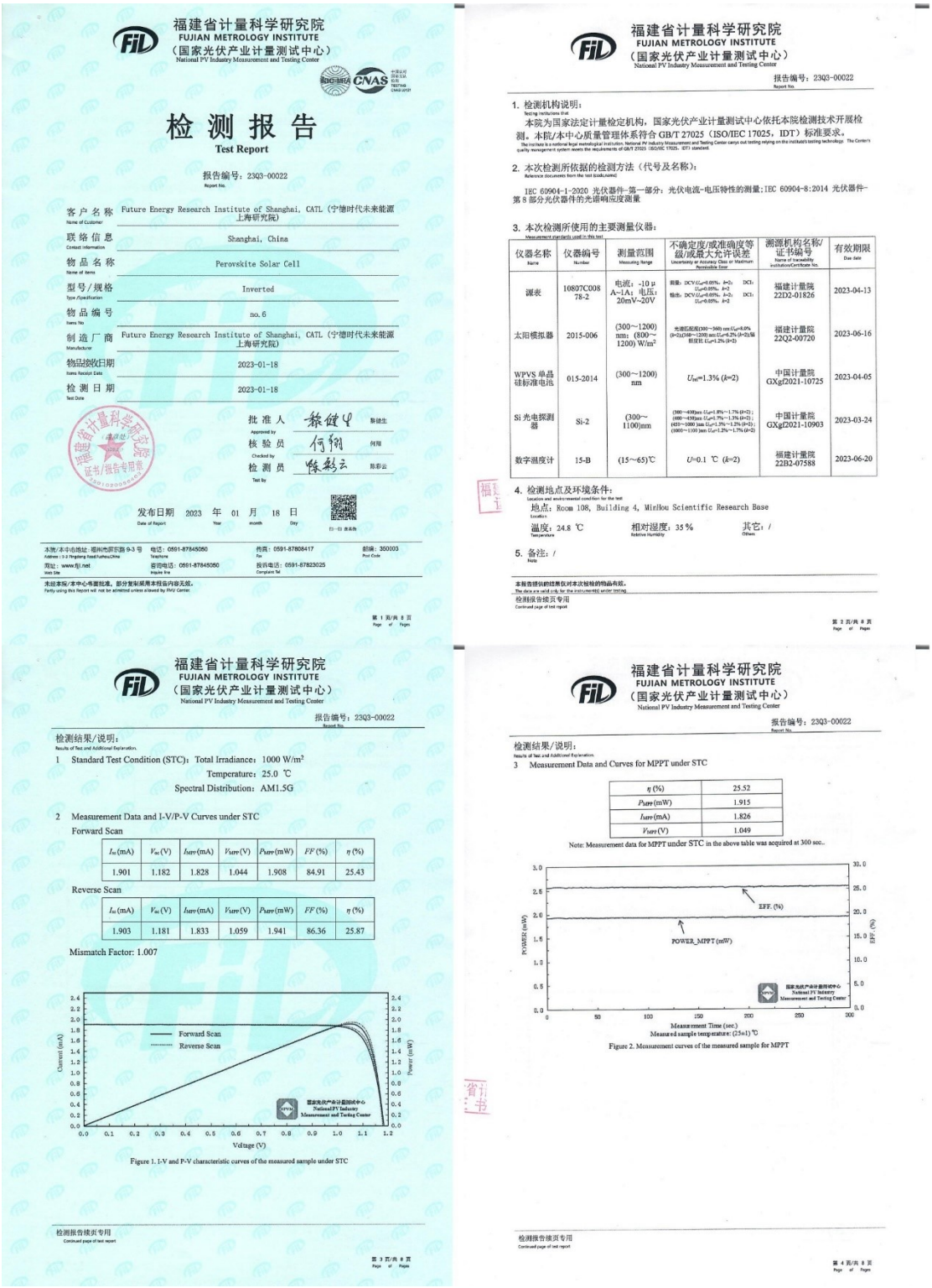
福建省计量科学研究院
FUJIAN METROLOGY INSTITUTE
（国家光伏产业计量测试中心）
National PV Industry Measurement and Testing Center

检 测 报 告
Test Report

报告编号：23Q3-00022

客户名称 Name of Customer	Future Energy Research Institute of Shanghai, CATL（宁德时代未来能源上海研究院）
联络信息 Contact Information	Shanghai, China
物品名称 Name of Items	Perovskite Solar Cell
型号/规格 Type /Specification	Inverted
物品编号 Items No.	no. 6
制造厂商 Manufacturer	Future Energy Research Institute of Shanghai, CATL（宁德时代未来能源上海研究院）
物品接收日期 Items Receipt Date	2023-01-18
检测日期 Test Date	2023-01-18

批准人 Approved by 黎健生
核验员 Checked by 何翔
检测员 Test by 陈彩云

发布日期 Date of Report 2023 年 Year 01 月 month 18 日 Day

本院/本中心地址：福州市群众路 9-3 号 电话 Telephone：0591-87845050 传真 Fax：0591-87808417 邮编 Post Code：350003
网址 Web Site：www.fjjl.net 咨询电话 Inquire line：0591-87845050 投诉电话 Complaint Tel：0591-87823025

未经本院/本中心书面批准，部分复制使用本报告内容无效。
Partly using this Report will not be admitted unless allowed by FMV Center.

第 1 页/共 8 页 Page of Pages

福建省计量科学研究院
FUJIAN METROLOGY INSTITUTE
（国家光伏产业计量测试中心）
National PV Industry Measurement and Testing Center

报告编号：23Q3-00022

1. 检测机构说明：
Testing institutions brief
本院为国家法定计量检定机构，国家光伏产业计量测试中心依托本院检测技术开展检测。本院/本中心质量管理体系符合 GB/T 27025（ISO/IEC 17025，IDT）标准要求。
The institute is a national legal metrological institution. National PV Industry Measurement and Testing Center carries out testing relying on the institute's testing technology. The Center's quality management system meets the requirements of GB/T 27025（ISO/IEC 17025，IDT）standard.

2. 本次检测所依据的检测方法（代号及名称）：
Reference documents from the test is conducted
IEC 60904-1-2020 光伏器件-第一部分：光伏电流-电压特性的测量；IEC 60904-8:2014 光伏器件-第 8 部分光伏器件的光谱响应度测量

3. 本次检测所使用的主要测量仪器：
Measurement standards used in this test

仪器名称 Name	仪器编号 Number	测量范围 Measuring Range	不确定度/或准确度等级/或最大允许误差 Uncertainty or Accuracy Class or Maximum Permissible Error	溯源机构名称/证书编号 Name of traceability institution/Certificate No.	有效期限 Due date
源表	10807C00878-2	电流：-10 μA~1A；电压：20mV~20V	源表：DCV U_{rel}=0.05%，k=2；DCI：U_{rel}=0.05%，k=2 输出：DCV U_{rel}=0.05%，k=2；DCI：U_{rel}=0.05%，k=2	福建计量院 22D2-01826	2023-04-13
太阳模拟器	2015-006	(300～1200) nm；(800～1200) W/m²	光谱匹配度(300～360) nm U_{rel}=8.0%（k=2）；(360～1200) nm U_{rel}=0.2%（k=2）；辐照度 U_{rel}=1.2%（k=2）	福建计量院 22Q2-00720	2023-06-16
WPVS 单晶硅标准电池	015-2014	(300～1200) nm	U_{rel}=1.3%（k=2）	中国计量院 GXgf2021-10725	2023-04-05
Si 光电探测器	Si-2	(300～1100)nm	(300～400)nm U_{rel}=1.8%～1.7%（k=2）；(400～430)nm U_{rel}=1.7%～1.3%（k=2）；(435～1000)nm U_{rel}=1.3%～1.2%（k=2）；(1000～1100)nm U_{rel}=1.2%～1.7%（k=2）	中国计量院 GXgf2021-10903	2023-03-24
数字温度计	15-B	(15～65)℃	U=0.1 ℃（k=2）	福建计量院 22B2-07588	2023-06-20

4. 检测地点及环境条件：
Location and environmental condition for the test
地点：Room 108, Building 4, Minhou Scientific Research Base
温度：24.8 ℃ Temperature 相对湿度：35 % Relative Humidity 其它：/ Others

5. 备注：/ Note

本报告提供的结果仅对本次被检的物品有效。
The data are valid only for the instrument(s) under testing.
检测报告续页专用
Continued page of test report

第 2 页/共 8 页 Page of Pages

福建省计量科学研究院
FUJIAN METROLOGY INSTITUTE
（国家光伏产业计量测试中心）
National PV Industry Measurement and Testing Center

报告编号：23Q3-00022

检测结果/说明：
Results of Test and Additional Explanation.

1 Standard Test Condition (STC)：Total Irradiance：1000 W/m²
Temperature：25.0 ℃
Spectral Distribution：AM1.5G

2 Measurement Data and I-V/P-V Curves under STC

Forward Scan

I_{sc} (mA)	V_{oc} (V)	I_{MPP} (mA)	V_{MPP} (V)	P_{MPP} (mW)	FF (%)	η (%)
1.901	1.182	1.828	1.044	1.908	84.91	25.43

Reverse Scan

I_{sc} (mA)	V_{oc} (V)	I_{MPP} (mA)	V_{MPP} (V)	P_{MPP} (mW)	FF (%)	η (%)
1.903	1.181	1.833	1.059	1.941	86.36	25.87

Mismatch Factor: 1.007

Figure 1. I-V and P-V characteristic curves of the measured sample under STC

检测报告续页专用
Continued page of test report

第 3 页/共 8 页 Page of Pages

福建省计量科学研究院
FUJIAN METROLOGY INSTITUTE
（国家光伏产业计量测试中心）
National PV Industry Measurement and Testing Center

报告编号：23Q3-00022

检测结果/说明：
Results of Test and Additional Explanation.

3 Measurement Data and Curves for MPPT under STC

η (%)	25.52
P_{MPP} (mW)	1.915
I_{MPP} (mA)	1.826
V_{MPP} (V)	1.049

Note: Measurement data for MPPT under STC in the above table was acquired at 300 sec..

Measured sample temperature: (25±1) ℃

Figure 2. Measurement curves of the measured sample for MPPT

检测报告续页专用
Continued page of test report

第 4 页/共 8 页 Page of Pages

Fig. S27. Independent PCE certification for Inverted PDI-treated PSCs of a small area (0.075 cm^2) at FuJian Metrology Institute (National PV Industry Measurement and Testing Center). The certified efficiency is 25.87% under reverse scan (I_{sc} of 1.903 mA, V_{oc} of 1.181 V and FF of 86.36%). The quasi-steady-state efficiency is 25.52% under

maximum power point tracking measured by National PV Industry Measurement and Testing Center.

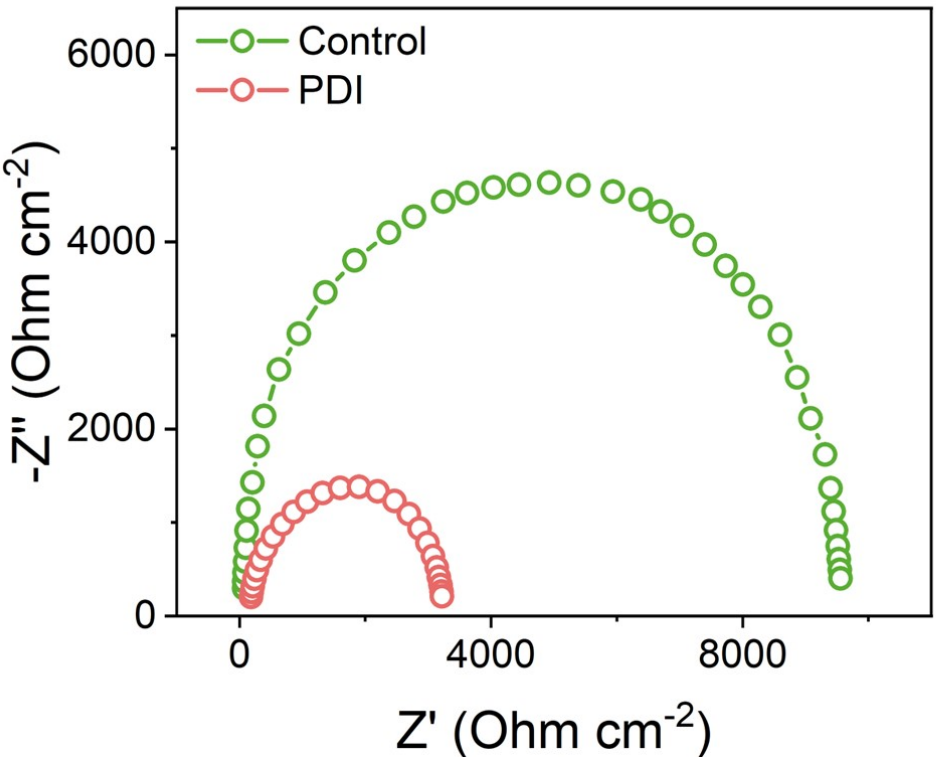

Fig. S28. Nyquist plots of Control and PDI-treated PSCs.

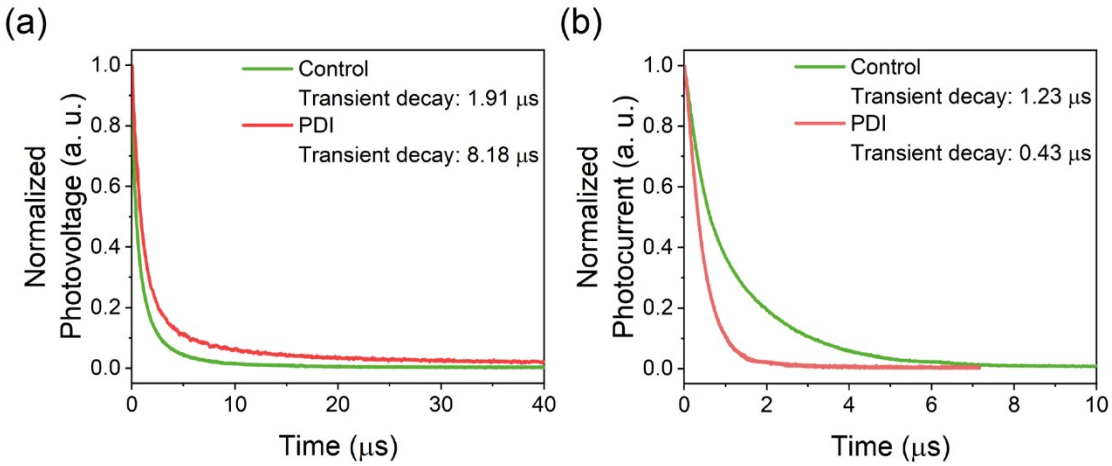

Fig. S29. (a) TPV and (b) TPC of Control and PDI-treated PSCs.

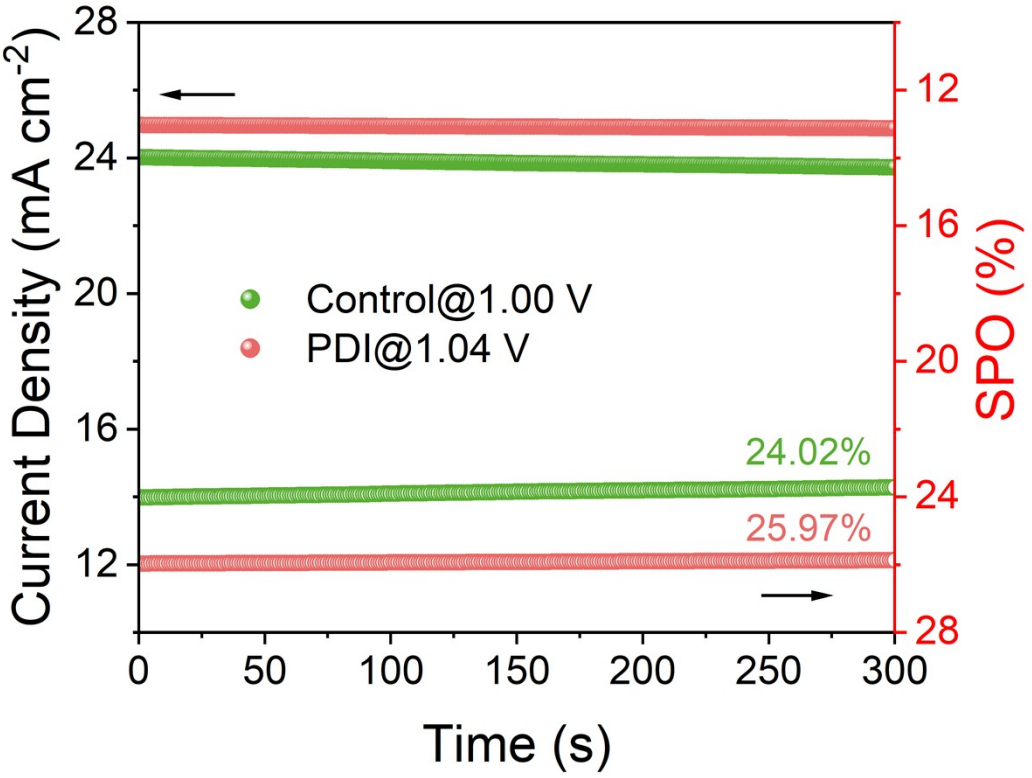

Fig. S30. The current density and steady power output measured at the maximum power point for 300 s of Control and PDI-treated PSCs.

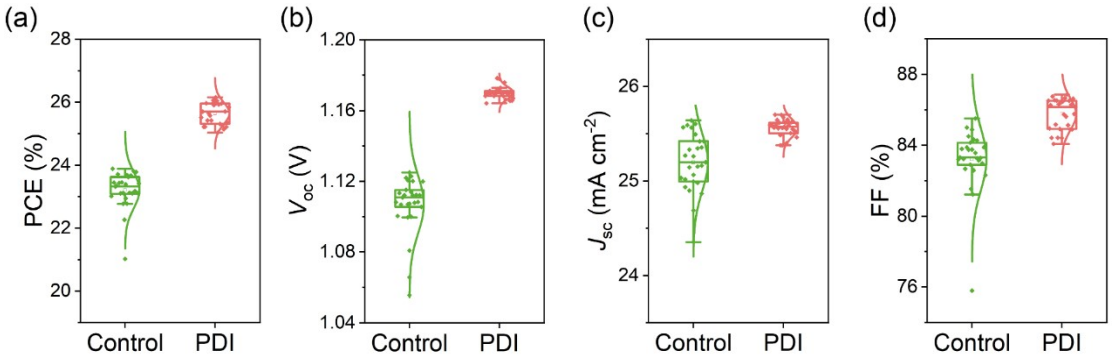

Fig. S31. Statistical distribution of PCE, V_{oc}, J_{sc}, and FF for 27 Control and PDI-treated PSCs.

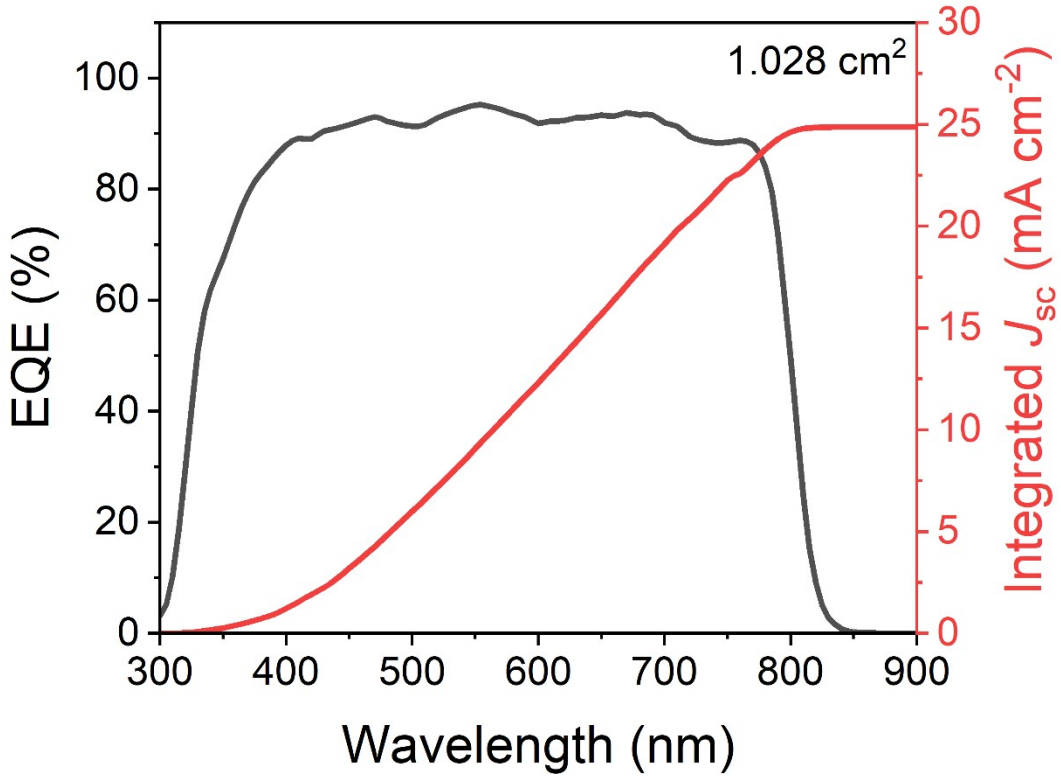

Fig. S32. EQE spectra and integrated J_{sc} of PDI-treated device with 1.028 cm^2.

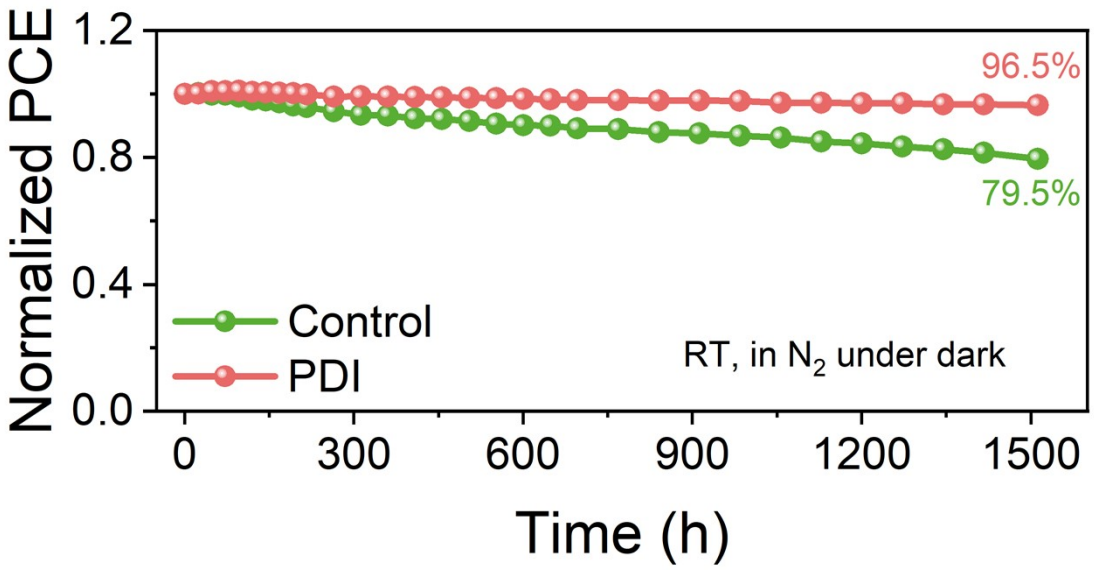

Fig. S33. Long-term storage stability of the unencapsulated Control and PDI-treated devices stored in a dark nitrogen environment.

Table S1. Photovoltaic parameters of Pip- and PI-treated devices.

Sample	Scan	V_{oc} (V)	J_{sc} (mA cm^{-2})	FF (%)	PCE (%)
Pip	Reverse	1.164	24.69	81.87	23.53
	Forward	1.156	24.58	81.84	23.25
PI	Reverse	1.163	25.16	83.98	24.28
	Forward	1.163	24.93	82.43	23.88

Table S2. Summary of the highest reported parameters of inverted PSCs.

Reference	E_g/eV	V_{oc}/V	J_{sc}/mA cm^{-2}	FF/%	PCE/%
J. Am. Chem. Soc., 2020, 142, 20134-20142[7]	1.54	1.17	24.92	80.17	23.37
Sci. Adv., 2021, 7, eabe8130[8]	1.55	1.17	23.9	83.6	23.4
Joule, 2022, 6, 2849-2868[9]	1.55	1.17	24.95	83.31	24.32
Science, 2022, 376, 416-420[10]	1.55	1.18	25.68	82.32	25.0
Science, 2022, 376, 73-77[11]	1.55	1.20	24.7	82	24.3
Nat. Photon., 2022, 16, 352-358[12]	1.56	1.15	24.9	83.46	23.91
Nature, 2022, 611, 278-283[13]	1.53	1.15	26.13	84.6	25.49
Science, 2022, 375, 434-437[14]	1.56	1.19	24.8	82.9	24.3
Science, 2023, 380, 404-409[15]	1.56	1.21	24.78	84.65	25.39
Science, 2023, 379, 683-690[16]	1.55	1.21	25.08	84.37	25.56
Nature Energy, 2023, 8, 462-472[17]	1.55	1.19	24.78	83.07	24.50
This work (0.075 cm^2)	1.55	1.18	25.67	86.47	26.15 (Certified: 25.87)
This work (1.028 cm^2)	1.55	1.18	25.00	82.12	24.18

References:

1. J. P. Perdew, K. Burke and M. Ernzerhof, *Phys. Rev. Lett.*, 1996, **77**, 3865-3868.
2. G. Kresse and D. Joubert, *Phys. Rev. B*, 1999, **59**, 1758-1775.
3. H. J. Monkhorst and J. D. Pack, *Phys. Rev. B*, 1976, **13**, 5188-5192.
4. M. B. Price, J. Butkus, T. C. Jellicoe, A. Sadhanala, A. Briane, J. E. Halpert, K. Broch, J. M. Hodgkiss, R. H. Friend and F. Deschler, *Nat. Commun.*, 2015, **6**, 1-8.
5. Y. Yang, D. P. Ostrowski, R. M. France, K. Zhu, J. van de Lagemaat, J. M. Luther and M. C. Beard, *Nat. Photonics*, 2016, **10**, 53-59.
6. P. Caprioglio, M. Stolterfoht, C. M. Wolff, T. Unold, B. Rech, S. Albrecht and D. Neher, *Adv. Energy Mater.*, 2019, **9**, 1901631.

7. F. Li, X. Deng, F. Qi, Z. Li, D. Liu, D. Shen, M. Qin, S. Wu, F. Lin, S.-H. Jang, J. Zhang, X. Lu, D. Lei, C.-S. Lee, Z. Zhu and A. K. Y. Jen, *J. Am. Chem. Soc.*, 2020, **142**, 20134-20142.
8. S. Chen, X. Xiao, H. Gu and J. Huang, *Sci. Adv.*, 2021, **7**, eabe8130.
9. Z. Zhu, K. Mao, K. Zhang, W. Peng, J. Zhang, H. Meng, S. Cheng, T. Li, H. Lin, Q. Chen, X. Wu and J. Xu, *Joule*, 2022, **6**, 2849-2868.
10. Z. Li, B. Li, X. Wu, S. A. Sheppard, S. Zhang, D. Gao, N. J. Long and Z. Zhu, *Science*, 2022, **376**, 416-420.
11. R. Azmi, E. Ugur, A. Seitkhan, F. Aljamaan, A. S. Subbiah, J. Liu, G. T. Harrison, M. I. Nugraha, M. K. Eswaran, M. Babics, Y. Chen, F. Xu, T. G. Allen, A. U. Rehman, C.-L. Wang, T. D. Anthopoulos, U. Schwingenschlogl, M. De Bastiani, E. Aydin and S. De Wolf, *Science*, 2022, **376**, 73-77.
12. H. Chen, S. Teale, B. Chen, Y. Hou, L. Grater, T. Zhu, K. Bertens, S. M. Park, H. R. Atapattu, Y. Gao, M. Wei, A. K. Johnston, Q. Zhou, K. Xu, D. Yu, C. Han, T. Cui, E. H. Jung, C. Zhou, W. Zhou, A. H. Proppe, S. Hoogland, F. Laquai, T. Filleter, K. R. Graham, Z. Ning and E. H. Sargent, *Nat. Photonics*, 2022, **16**, 352-358.
13. Q. Jiang, J. Tong, Y. Xian, R. A. Kerner, S. P. Dunfield, C. Xiao, R. A. Scheidt, D. Kuciauskas, X. Wang, M. P. Hautzinger, R. Tirawat, M. C. Beard, D. P. Fenning, J. J. Berry, B. W. Larson, Y. Yan and K. Zhu, *Nature*, 2022, **611**, 278-283.
14. X. Li, W. Zhang, X. Guo, C. Lu, J. Wei and J. Fang, *Science*, 2022, **375**, 434-437.
15. S. Zhang, F. Ye, X. Wang, R. Chen, H. Zhang, L. Zhan, X. Jiang, Y. Li, X. Ji, S. Liu, M. Yu, F. Yu, Y. Zhang, R. Wu, Z. Liu, Z. Ning, D. Neher, L. Han, Y. Lin, H. Tian, W. Chen, M. Stolterfoht, L. Zhang, W.-H. Zhu and Y. Wu, *Science*, 2023, **380**, 404-409.
16. W. Peng, K. Mao, F. Cai, H. Meng, Z. Zhu, T. Li, S. Yuan, Z. Xu, X. Feng, J. Xu, M. D. McGehee and J. Xu, *Science*, 2023, **379**, 683-690.
17. X. Zheng, Z. Li, Y. Zhang, M. Chen, T. Liu, C. Xiao, D. Gao, J. B. Patel, D. Kuciauskas, A. Magomedov, R. A. Scheidt, X. Wang, S. P. Harvey, Z. Dai, C. Zhang, D. Morales, H. Pruett, B. M. Wieliczka, A. R. Kirmani, N. P. Padture, K. R. Graham, Y. Yan, M. K. Nazeeruddin, M. D. McGehee, Z. Zhu and J. M. Luther, *Nat. Energy*, 2023, **8**, 462-472.